Wind-driven Modification of Small Bedforms in Gusev Crater, Mars

by

Mary Pendleton-Hoffer

A Thesis Presented in Partial Fulfillment
of the Requirements for the Degree
Master of Science

Approved July 2016 by the
Graduate Supervisory Committee:

Philip Christensen, Chair
Kelin Whipple
L. Paul Knauth

ARIZONA STATE UNIVERSITY

August 2016

ABSTRACT

The Spirit landing site in Gusev Crater has been imaged by the Mars Reconnaissance Orbiter High Resolution Imaging Science Experiment (HiRISE) camera more than thirty times since 2006. The breadth of this image set allowed a study of changes to surface features, covering four Mars years.

Small fields of bedforms comprised of dark material, and dark dust devil tracks are among the features revealed in the images. The bedforms are constrained within craters on the plains, and unconstrained in depressions less than 200m wide within the topography of the Columbia Hills, a ~120m-high structure in center of Gusev. Dust devil tracks appear in many images of the bedforms.

Within the Columbia Hills, three bedform fields approximately 180m^2 and composed of fine dark basaltic sand were studied, using five HiRISE images taken from 2006 to 2014. Both bedform crests and the dust devil tracks superimposed on them were evaluated for change to azimuth and length, and for correlation between the features. The linear to slightly sinuous transverse crests ranging from less than 1m to 113m in length and two to three meters in wavelength, are primary bedforms. During the study they shifted as much as 33 degrees in azimuth, and individual crests moved on the surface as much as 0.75m. The greatest changes corresponded to a global dust storm in 2007. Average crest movement was documented at the rate of 0.25m per year. Rather than moving progressively, the crests eventually returned to near their original orientation after the storm. The dust devil tracks, reflecting a more complex wind regime, including

vortex development during diurnal heating, maintained predominantly NW-SE orientations but also reflected the effects of the storm.

The observed modifications were neither progressive, nor strictly seasonal. The apparent stability of the bedform geometry over four seasons supports the predictions of the Mars Regional Atmospheric Modeling System (MRAMS): low speed (1-7.5 ms^{-1}), daily alternating winds of relatively equal force. Crest profiles were found to be nearly symmetrical, without slipfaces to indicate a preferential wind direction; this finding also is supported by the MRAMS model.

DEDICATION

Dr. Edmund Stump, whose vivid enthusiasm inspired me with rocks on Earth;

Dr. Ronald Greeley, whose imagination and experience inspired me with rocks in space;

Family and friends, who encouraged a pianist becoming a

geologist;

And my husband, Warren Hoffer, glorious tenor and musician,

greatest friend and supporter –

I would not be here, and this would not happen, without you.

ACKNOWLEDGMENTS

Thanks are due to so many people who contributed to the completion of this project. Dr. Phil Christensen, who took on Chairmanship of my Advisory Committee after the death of my advisor and mentor, Dr. Ronald Greeley, and Dr. Kelin Whipple and Dr. Paul Knauth, who kindly joined the committee, have been truly supportive and generous with their time and counsel. David Nelson has been truly exceptional, donating many hours to construct the ArcGIS, GMT and other software programs I needed, and teaching me to use them. Dan Ball produced a fine set of photographic prints of the study areas at the initial stage of the work. David Williams and Stephanie Holaday have provided an array of logistical supports. The two administrative Rebeccas - Dial and Polley - have kept me moving in the right academic direction. Current and former colleagues, Amy Zink, Ramses Ramirez, Leon Manfredi, Rebekah Kienenberger, Melissa Bunte, Patrick Whelley, Lynn Neakrase, Devin Waller, Enzo Cataldo, Kyle Mohr and Kyle Guzman, have acted as sounding boards for my ideas, and frequently as computer support. Meg Hufford has brightened long days. I extend my sincere gratitude to you all.

TABLE OF CONTENTS

CHAPTER Page

LIST OF TABLES

Table Page

LIST OF FIGURES

Figure Page

Chapter 1

INTRODUCTION

Gusev Crater, at 175^{o}E, -14^{o}S, is approximately 160 km in diameter, lies at the margin of the Mars highlands and the northern lowlands. Two large features are nearby: Ma'adim Vallis, an 800km channel leading north from the highlands, which "flows" to the crater, and Apollinaris Patera, an inactive volcano 200km to its north.

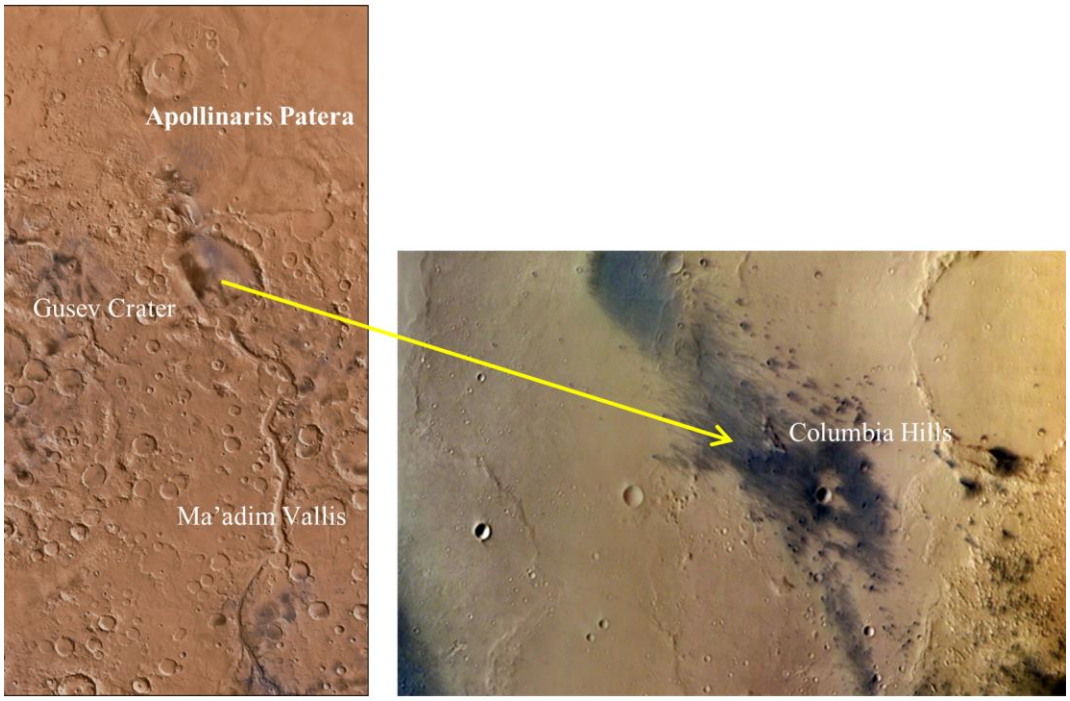

Figure 1. Gusev Crater and the Columbia Hills. The Hills are within a wind-swept, dust-freed area showing the direction of prevailing daytime winds . *(Viking Global Map and THEMIS/HRSC)*

Spirit, one of two roving instrument suites sent to Mars in 2004, landed on the surface of Gusev Crater in January (Squyres, 2004). It landed near an outcrop, the Columbia Hills, and during its four-year traverse it passed into these Hills, taking a variety of measurements, before coming to its final resting point at Home Plate (Figure 2). One of the features Spirit examined during its journey was the small, dark El Dorado "dune"

field. While it was observing the field, wind-caused change in the bedform crest orientation was seen (Sullivan, 2008).

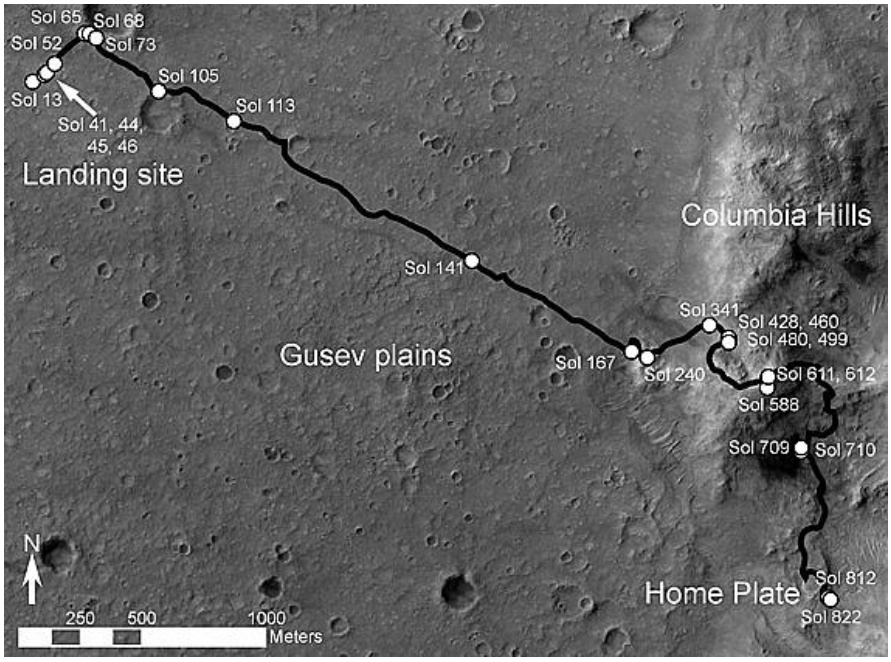

Figure 2. The Spirit traverse map. Spirit traveled from the landing site to Home Plate. Spirit visited El Dorado during Sols 706-711. *(Journal of Geophysical Research: Planets, 116, E7, E00F22*, 22 APR 2011 DOI: 10:1029/2010JE003712.*)*

The early missions to Mars, produced little evidence of sand movement on the surface (Edgett and Malin, 2000; Zimbelman, 2000, Fenton, 2005; Bourke, 2008, Bridges, 2007). Yet many large dune fields, among other aeolian features, were observed on the surface, both from landers (Viking and Pathfinder) and orbiters (Viking and Mars Global Surveyor). Concurrent to the Mars Exploration Rover (MER) missions, the Mars Reconnaissance Orbiter (MRO), with its High Resolution Imaging Science Experiment camera (HiRISE) (McEwen, 2007), collected repeat images of the rovers' locations, both to record and help direct their progress, and, as the project advanced, to collect data on transient aeolian features common in the areas: for Gusev Crater, that meant dust devil

tracks (Greeley, 2004, 2004a, 2006), and wind streaks, yardangs and granular surface deposits (Grant, 2004; Sullivan, 2008). Using the multiple imaging of MRO and HiRISE, and often in conjunction with Viking and Pathfinder data, recent research has finally confirmed changes in large dune fields such as Rabe and Gale Craters (Fenton, 2006; Hobbs, 2010; Silvestro, 2013).

Many small craters within Gusev Crater contain small dunes of loose, dark material. In addition to El Dorado, three dark fields of bedforms are located in the Columbia Hills; all are in depressions, but unconstrained by crater rims. By studying the repeat image coverage of these small features, it could be possible to determine (1) if change due to wind is occurring, (2) to infer the predominant wind directions involved in that change, and (3) if the change is seasonal and repetitive, or progressive.

BACKGROUND

Mars's surface shows abundant variety of aeolian features: dunes and dune fields, and bright and dark streaks associated with broad topographic highs, small boulders or dust devil tracks. The frequency of these features was anticipated before Mariner 9 and seen by it and every subsequent martian orbiter and lander (Sagan, 1972; Malin, 1998).

Dust and Sand Conundrum. Winds on Mars are known for raising dust, enough to create frequent global dust storms (Edgett and Malin, 2000; Greeley, 2000; Golitsyn, 1973; Sagan, 1969, 1972). On Mars, as on Earth, winds with the velocity sufficient to saltate sand and ultimately create bedforms do not need to be as high as those required to entrain dust (Greeley and Iversen, 1985). To lift dust, wind velocity must be sufficient to

overcome the resistance presented by a number of factors such as surface pressure, ground temperatures, roughness height, atmospheric stability, particle density and diameter, and the strength of cohesive forces among particles (Greeley and Iversen, 1985; Pollack, 1976). For Mars, with much lower gravity and atmospheric density than Earth, it should be more difficult to move these materials, even with exceptionally high estimated threshold wind speeds, between 50 and 100 ms^{-1} (Pollack, 1976). Gierasch (1968) anticipated extreme winds of 100-140ms^{-1}, and easy transport of dust particles. Wind tunnel studies found lower speeds, although the Mars threshold was still 10 times the terrestrial one (Greeley and Iverson, 1985; Greeley, 2000). The Viking and Pathfinder landers found actual continuous wind speeds to be very low, even as little as 1 ms^{-1} (Sullivan, 2000). During the Viking Landers' mission (arriving in 1976), there was no observable sand movement over a six year period, and after Pathfinder (1996), dunes were called 'inactive' (Zimbelman, 2000). Since both large sand seas and smaller bedforms have been documented (Fenton and Hayward, 2010; Greeley, 2006; Malin, 1998; Sagan, 1972), the question of how winds strong enough to lift and suspend significant amounts of dust and create frequent regional dust storms can fail to move what should be more easily saltated sand, has been the focus of much research.

With the production of large data sets of high resolution images by Mars Global Surveyor's Mars Orbiter Camera (MOC) and Mars Reconnaissance Orbiter's HiRISE, repeat coverage of surfaces such as the locations of the two rovers (Opportunity and Spirit), and the Phoenix lander, has been possible. Research using these data sets has presented several likely examples of sand movement (Balme, 2008; Bandeira, 2010;

Bourke, 2008; Chojnacki, 2010; Silvestro, 2010). In addition, modeling research has shown that threshold speeds may be lower, and saltation trajectories may be higher than previously believed (Kok, 2010).

Dust and Dust Devils. Data coming from the Spirit rover have provided ground truth regarding dust. It is continually dropping from the atmosphere (Landis, 1996) and the rovers' solar panels are constantly covered in dust. Sagan (1969) expected dust to be lifted high into the atmosphere by dust devils, contributing to the formation of the global dust storms. That dust devils do lift dust was proven in 2005: the solar panels on Spirit were performing poorly due to the dust accumulation when a dust devil passed over the panels, clearing them of the dust (David, 2005). Spirit instruments observed the surface before and after the passage of a dust devil and found dust had been removed by the vortex (Greeley, 2005). Dust devils generally leave a dark streak behind them on the martian surface. They can provide a visible diagnostic tool for determining wind direction, since they move in the direction of the horizontal air flow (Greeley, 2004a). Greeley (2006, 2010) also presented evidence of active dust devils in the plains west of the Columbia Hills, noting the importance of directional azimuths.

Figure 3. Dust devil in Gusev Crater. One of hundreds imaged during the Spirit mission in Gusev crater *(MER Spirit image, sol 581, NASA/JPL/Cornell).*

Sand and Bedforms. The occurrence of ubiquitous sand dunes on Mars' surface provides evidence that, as on Earth, saltation, described by Bagnold (1954) as a principle factor of movement, is the dominant mode of sand transport on Mars (Parteli, 2009). The transport of sand on Mars is thought to occur only occasionally (a few times a decade), when storms create strong gusts of wind reaching velocities 10 times greater than occur on Earth. When particles saltate on Mars, they should do so at lower speeds and with a longer trajectory than on Earth, creating features with greater wavelength than comparable features on Earth (Kok, 2010).

When Spirit visited the dark field, El Dorado, in the Columbia Hills, a variety of measurements were taken, including overturning the soil with one wheel to allow examination below the surface (Sullivan, 2008). The surface particles were found to be basaltic in composition and to range in size from 100 to 300 microns, i.e. fine basaltic

sand. Spirit also observed the passage of a dust devil over the bedform; a darker surface track was left behind.

Extensive dune fields were first identified in the Mariner 9 data (Sagan, 1972). The Planetary Dunes Workshop created a database of the large martian dune fields which catalogs the comparable and contrasting characteristics, frequently linked to latitude (Hayward, 2008; Bourke, 2010; Hayward, 2014). Some large dunes, called transverse aeolian ridges (TARs), are isolated on the martian plains (Balme, 2008; Zimbelman, 2010). Instead of asymmetric lee and stoss slipfaces, they are nearly symmetrical in cross section, often appear as a single, or as a few, widely-separated crests, and show no evidence of recent movement (Bridges, 2012). Intracrater bedforms have recently been shown to indicate wind direction (Kienenberger, 2011) and may serve as models for the Columbia Hills bedforms.

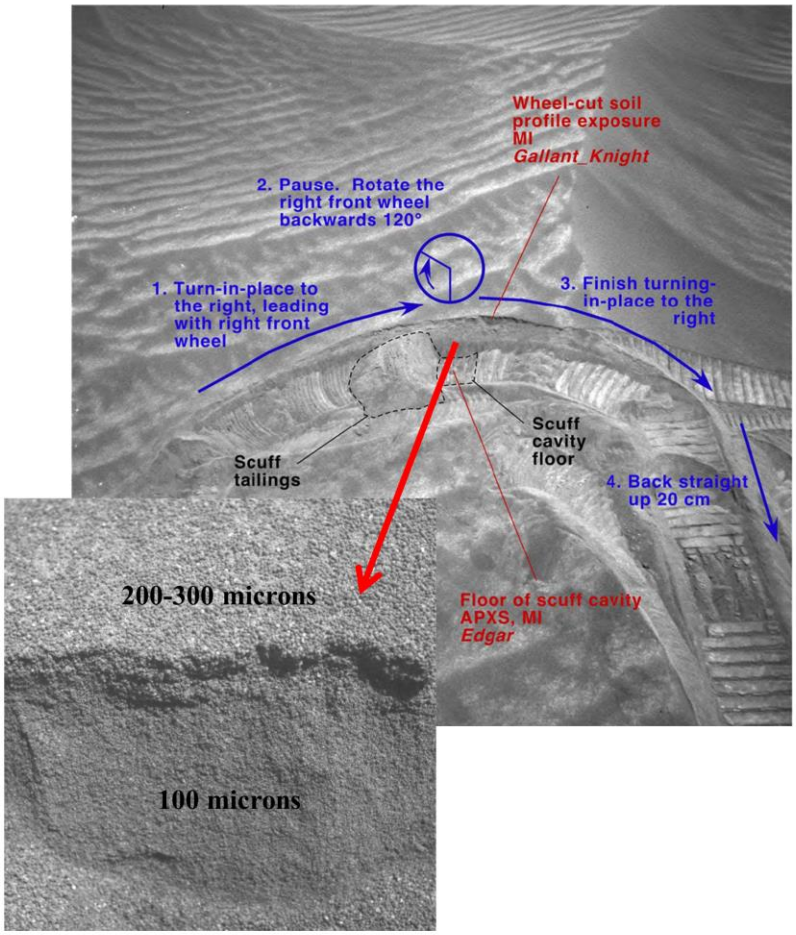

(Journal of Geophysical Research: Planets
113, E6, E06S07, 19 JUN 2008 DOI: 10.1029/2008JE003101)

Figure 4. Spirit's investigation of the surface of El Dorado. The material was loose enough to fall into the small trench dug by a wheel. Secondary ripples run perpendicular to the bedform crests.

Atmospheric Circulation Models. Gierasch (1971) found that topographic relief increases the mean winds on Mars by factors of two to three over those occurring in absence of topographic elevations. Wilson (1971) found that changes to terrestrial dunes occur with changes in local wind speeds, typically near topographic highs, similar to the

Columbia Hills. Dune patterns on Mars are partially controlled by topography (Breed, 1979); in addition, Mars has high relief that encourages katabatic winds.

Several atmospheric circulation models have been proposed for Mars. The NASA Ames General Circulation Model (GCM) was developed from Earth models and adapted to Mars conditions (Haberle, 1993) with good results, given its low resolution (tens of km) relative to the size of dunes and dune fields. The Mars Regional Atmospheric Modeling System (MRAMS) developed by Rafkin (2001), is useful for this study because it predicts wind flow patterns in Gusev Crater at 14.5m above the surface over a 24-hour period, for days selected from each of the four seasons of a Mars year. It can, therefore account for seasonal variations. This model suggests that the martian atmosphere is 2-3 times more turbulent than the terrestrial atmosphere in the afternoon, but that flux is an order of magnitude smaller due to lower atmospheric density. It predicts the observed formation of dust devils within the crater. The model also indicates katabatic/anabatic flows: diurnal heat causes air to rise from the center of the crater and flow up out of it, while cooler nocturnal flow returns down, over the crater rim into the crater. Both actions appear to be enhanced by the valley feature, Ma'adim Vallis and the mountain, Apollinaris Patera. The MRAMS model is on a scale an order of magnitude larger than the Columbia Hills, but it is able to provide a general directional pattern and wind speeds that apply to the Hills. The hill structure, while only ~120 m high, also may alter the winds in more subtle ways (Wilson, 1971).

OBJECTIVE AND APPROACH

The objective of this research is to determine what change in the surface bedforms is occurring, and what the implications might be for understanding the wind patterns, as predicted in atmospheric models. This involves investigation of both bedforms and dust devil tracks. Azimuth and length are examined through use of geographic software which provides the correct registration of multiple images, and allows the determination of morphometric data, azimuth and length, for both observed feature types. A Digital Elevation Model (DEM) of the area exists; its pixel resolution is very close to that of the features to be examined, so it provides limited topographic information.

POTENTIAL CONTRIBUTIONS

The bedforms in the Columbia Hills are very small, only recently visible by the high resolution (average 0.25 – 0.3m/pixel) HiRISE images. This size feature has been described by other researchers as, "ripples," (Silvestro, 2010), "wind ripples," (Lapotre, 2016) and "dune ripples" (Ewing, 2016; Sullivan, 2008), and all of them are secondary to a larger, underlying dune. None of the previously studied "ripples" fit the definition of them as seen on Earth: asymmetrical linear bedforms of centimeter-size height and wavelength, with coarse grains on the crests and fine grains in the troughs. The Columbia Hills bedforms are very close in size to the HiRISE image resolution, but they are visible because of their linearity. They are an order of magnitude smaller than any free-standing bedform fields studied to date. In addition, the primary particle size, that of fine sand (~ 100 microns), is smaller than previously studied. The HiRISE images of this area cover a

period of approximately four Mars years (with the concluding image used in this study), allowing for observation of the features through time. This study of a mid-range element between the apparently easily lofted dust and the less easily saltated coarse sand of the larger dunes , with ~500 microns and greater particle size, (Fenton, 2006, Hobbs 2010), may contribute to the resolution of the dust-sand conundrum. The correlation of dust devil tracks with bedforms has previously not been studied.

Chapter 2

METHODS

STUDY AREA

The Columbia Hills, which lie to the east of the Spirit landing site, became part of the Spirit traverse, and a significant study of the eastern edge of one of the bedform areas was conducted. The Hills form a north-pointing, triangular-shaped feature, ~120 m in elevation, ~ 8.4 km by ~4.5 km in dimension, with slopes dipping south, 8-10 degrees. El Dorado, a field of dark bedforms, found near the center of the triangle, was examined after driving Spirit eight meters into the area and employing several of the instruments on board (Sullivan, 2008). Particle size was measured at 200-300 microns on the surface, and seen to be coarser at the crest of the bedform. The troughs could not be evaluated from Spirit's location. The majority of the particles below the unconsolidated surface were ~100 microns. Composed of mafic material, they were described as "basaltic sand." Because of the unconsolidated nature of the sand, the rover did not proceed further into the field. The height of the crests was estimated at ~0.3m and crest wavelength at ~2-3m. Comparison photographs taken during and at the end of the study showed some movement of the crests.

Dust devil tracks, obvious on the plains where Spirit landed, became a focus of studies, both directly from Spirit (Greeley, 2006; Waller, 2011) and from orbit (Verba, 2010). These transient features are identified primarily by albedo, since they have almost no topographic footprint. Dust devil tracks on the bedforms in the Columbia Hills were

previously unconfirmed, and provide an another level of information about the aeolian activity in this area.

BEDFORM STUDY

Four unconstrained areas of bedforms are visible in the Columbia Hills; three are named for their position, North Columbia Hills (NCH), South Columbia Hills (SCH) and East Columbia Hills (ECH), and the fourth, El Dorado (ED), was named by the Spirit team.

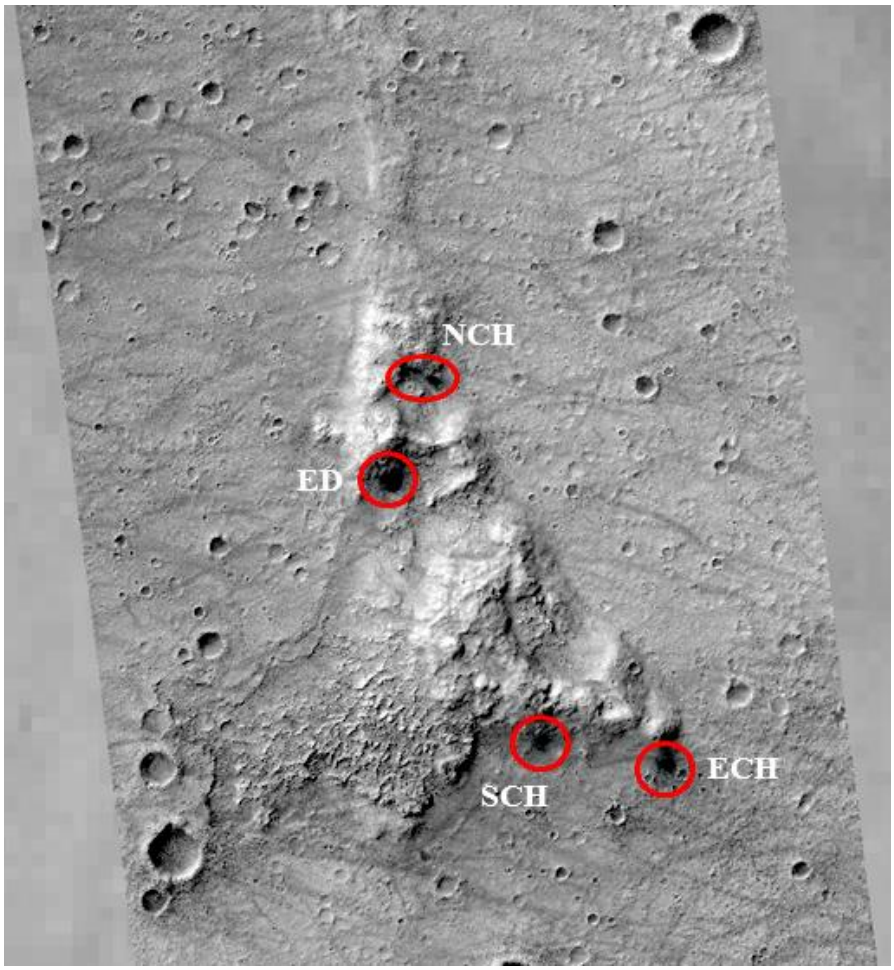

Figure 5. Bedform areas in the Columbia Hills (*HiRISE PSP_001513_1655*)

While monitoring the active Spirit, HiRISE took 22 images of the area; these images were taken with some control of phase and solar incidence angles for accuracy in imaging Spirit and its environment.

After the demise of Spirit, HiRISE has continued to image the area at least once an Earth year. This set of images is excellent for purposes of this study; five images (Table 1) were chosen to provide multi-seasonal variety as well as to surround the large global dust storm of 2007 (Wang and Richardson, 2015), and to include the first and one of the most recent images (2014). The earliest two images in the set, PSP_001513_1655 and PSP_001777_1650, were used to by USGS Astrogeology Science Center in Flagstaff (astrogeology.usgs.gov) to create a digital elevation model (DEM). The early images did not include the ECH area, and in order to include the first image in the set, the ECH area was eliminated from the study. The DEM was used, however, to confirm the general N-S dip of the slopes of the surface.

Table 1

Images Selected for the Study

Image	Date	Ls	Season	PA	IA	Resolution
ESP_037709_1650	8/12/2014	177.3	N Su	67.1	58/32	0.25
ESP_019301_1650	9/8/2010	145.2	N Su	55.9	61/29	0.25
PSP_009174_1650	7/11/2008	97.1	N Su	59.7	64.5/25.5	0.25
PSP_003689_1650	5/10/2007	235.46	N A	52.9	49.3/40.7	0.25
PSP_001513_1655	11/22/2006	139.13	N Su	73.6	60.3/29.7	0.25

*For the remainder of this paper, the image identifiers will be abbreviated to the non-zero number of image, i.e., 1513, 3689, 9174, 19301, 33709.

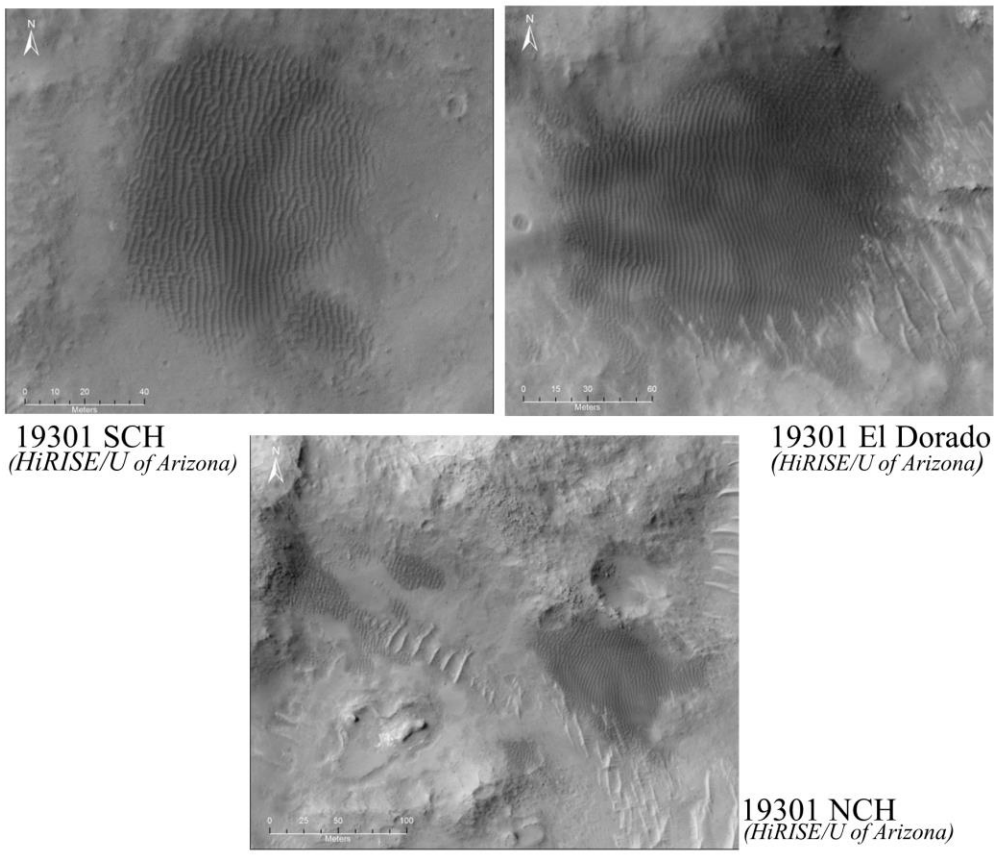

Figure 6. HiRISE and Spirit Images of the study areas. The N-S trend of dark bedforms is apparent, as are the darker dust devil tracks in each image. The bright bedforms (El Dorado and NCH) are endurated, dust-covered TARS (transient aeolian ridges). *(HiRISE image ESP_019301_1650)*

Since one goal was to determine if any noted change was seasonal or progressive, a variety of seasons (L_s) was chosen to control for possible repetition. One image per season would have been ideal, but proved impossible because of the difference in

resolution for a crucial image; ESP_0312611650, taken in northern winter, had resolution of 0.5m/pixel and could not be registered with the other images in the group. Both phase angle (PA, the angle between the sun, the camera and the surface) and incidence angle (IA, the angle between the sun and the surface) varied significantly. The phase angles were, however, close enough to register the images in the project to within one pixel of variance, equal to ~0.25 m surface distance. The incidence angles (IA) and sun heights (H) above the horizon were sufficient to make the topography of the small bedforms comfortably visible.

A global THEMIS infrared daytime mosaic (50m/pixel) was loaded into an ArcGIS project (created by Environment Systems Research Institute, http://www.esri.com); five HiRISE JPEG2000 images with 0.25m/pixel resolution were acquired from the website (http://hirise.lpl.arizona.edu), and co-registered in ArcGIS using surrounding rocks, small craters and bedrock for accurate reference. All images were illuminated from the left (west). The bedform crests were manually digitized (annotated), producing a line for each crest, all at 1:200 zoom (1 image cm: 200 ground cm). Bedform crest was defined as the juncture of bright pixel on the left and dark on the right, and using the darkest of the pixels when more than one pixel density was apparent.

Each area was digitized, producing ~ 400 data points for NCH, ~ 800 for ED, and ~ 300 for SCH, in each of the five images. ArcGIS allows for determination of both azimuth and length, which were the important characteristics, and the data was run for whole images, combining NCH, ED and SCH, as well as for those individual areas. Changes in the azimuth were recorded; the length of each orientation segment of a crest

line was calculated giving an average for each crest. While length was noted and included in production of Rose diagrams, it was also considered a check on the quality of annotation. Most of the visible crests showed ~N-S orientation.

After a review of the initial results, two further approaches were applied. First, a small group of crests in each image was selected, redigitized and evaluated (called Focus Boxes). The edges of the bedform, where, due to location and slope (Breed, 1979; Wilson, 1971) the movement of the features might be exaggerated by topographically modified winds were avoided. Second, two individual crests in each image, one on the east and one on the west side of each area, were chosen, digitized and compared.

DUST DEVIL TRACKS

There are many fewer dust devil tracks than crests in the bedform images. Their footprints, however, are much larger, and the orientations more extreme. They were digitized and evaluated in the same manner as the crests. The width of the track, which potentially might indicate the direction of the active dust devil (Greeley, 2004), was not considered here. Since dust devils are the product of daytime heating, in this case, of the plains to the west of the Columbia Hills, and because diurnal winds flow from the west and northwest, it was assumed that the dust devil tracks probably originated from the westerly direction, and could be digitized accordingly.

Chapter 3

RESULTS

BEDFORM CRESTS

The bedform crest study yielded four sets of data: (1) the combined azimuth per area for a complete image (three areas combined); (2) the crest data for each of the three areas, calculated separately; (3) the focus box data for each area; (4) the individual crests, two for each area. These results are presented in Tables 2, 3, 4, and 5.

Table 2.

Single Azimuth for Full Image (1)

Image	Azimuth	Avg Length (m)	Change (deg)
1513	17.8	8.4	NA
3689	4.2	8.2	W 13.5
9174	27.4	7.3	E 23.1
19301	15.1	8.4	W 12.3
37709	4.8	12.6	W 10.2

This set of data quantify the modification of the bedforms. The orientation change in degrees, while not large, reaches 6.4% between the second and third images, enough to validate the study. The change in azimuth is greatest for the third image, following the global dust storm. The first two and the last two images show similar correlation in azimuth values.

Figure 7 gives an example of the type of digitizing and the calculated results. The first image shows the digitization, the second a single azimuth derived from the set

(correlates to Table 2), and the third shows individual azimuth lines, which were averaged to produce a single azimuth for the area.

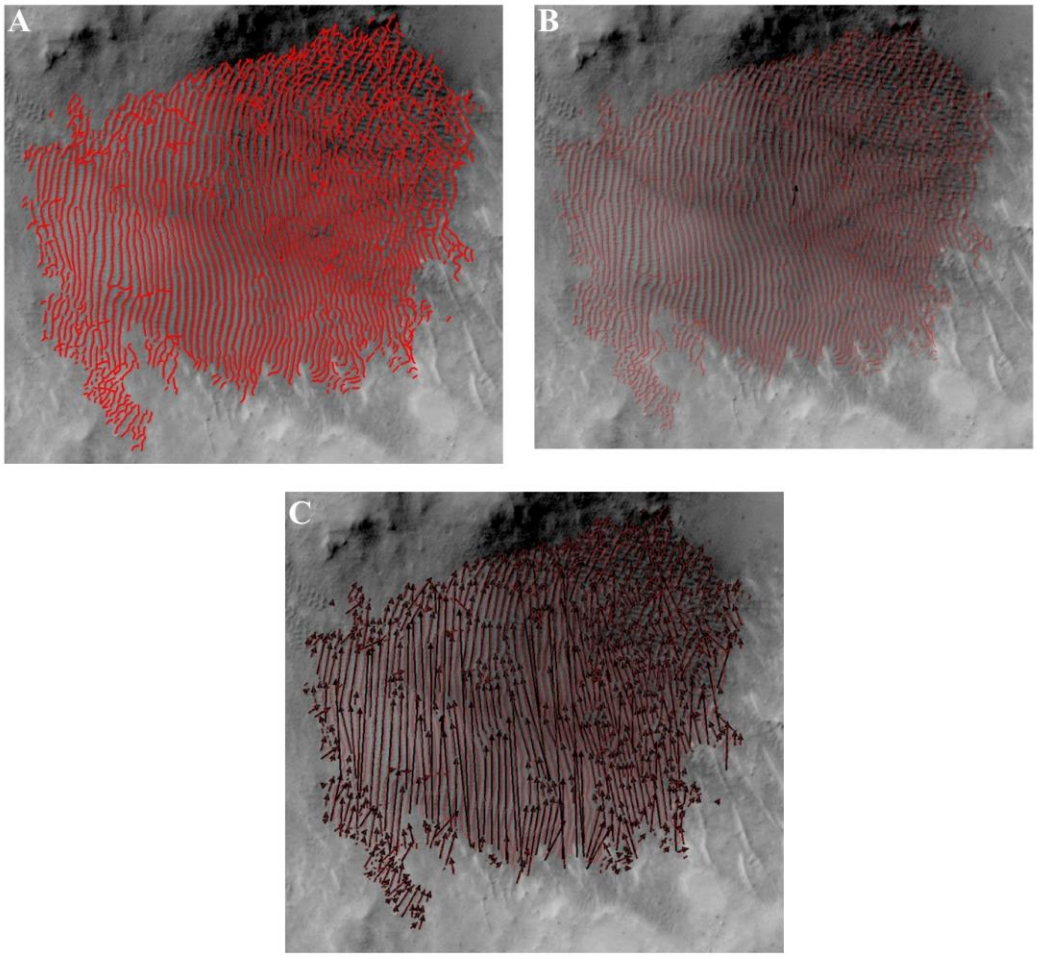

Figure 7. Example of annotated crests. El Dorado. A: all digitized crests; B: all crests with average azimuth (small black arrow); C: all crests with individual azimuth determinations. *(HiRISE image 1513)*

The crests were separated into area (NCH, ED, SCH) for the second data set. Smaller change was seen in this group than in the previous, since each area included a smaller data set of specific topography and wind. The change in orientation for all three areas is greatest between the second and third images; this, again, reflects the passage of

a global dust storm, which could have increased the winds by as much as an order of magnitude.

Figure 8 shows the digitized crests in El Dorado. The earliest images, 1513 and 3689 have many similarities, particularly in the center of the bedform, but also in the northeastern corner, where the linear crests are disrupted. The middle images, 9174 and 19301, both follow dust-raising events; the first after a global storm in 2007, and the second after a smaller, regional storm in 2009 (Wang and Richardson, 2015). These two images also have similarities to each other; there is more disruption in the center of the bedform than is seen in the early images, and the northeastern corner appears much more disrupted. The final image, 33709, taken more than three Earth years later, shows greater similarities with the earliest images.

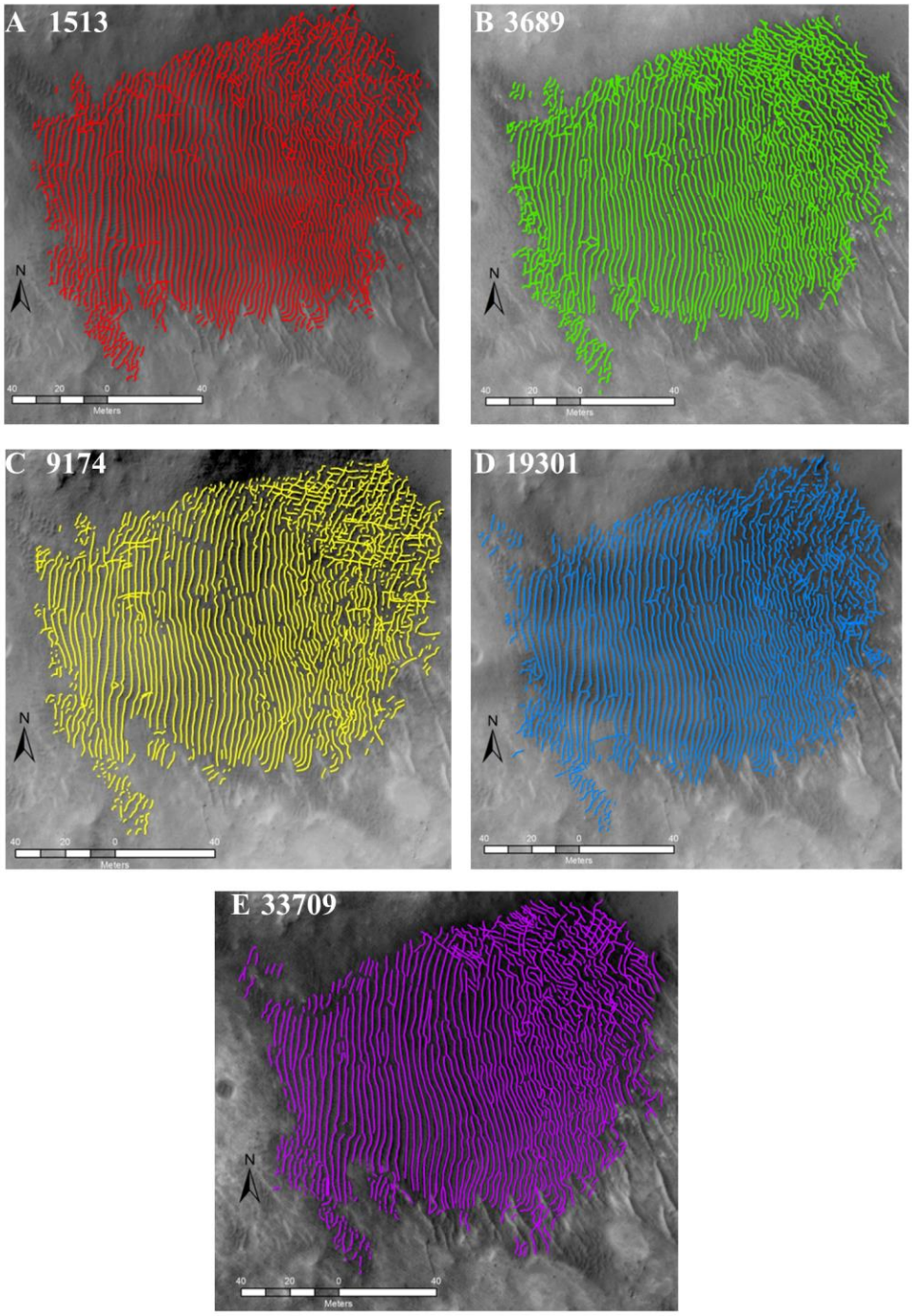

Figure 8. Digitized crests in El Dorado. A is the earliest image; C was taken after the global dust storm of 2007 and D after a regional storm in 2009; E is the final image of the set.

Table 3 shows azimuth data from the three areas. For NCH, the first and last images correlate well. For El Dorado and SCH, the second image compares well to the last.

Table 3.

All Crest Azimuths by Area (2)

Area and Image	Azimuth (deg)	Average Length (m)	Orientation Change (deg)
NCH 1513	20.5	10.4	NA
NCH 3689	10.6	6.8	W 9.9
NCH 9174	30.2	7.9	E 19.4
NCH 19301	24.4	6.5	W 5.8
NCH 33709	23.9	9.7	W 0.5
ED 1513	8.7	7.9	NA
ED 3689	353.3	9.5	W 15.4
ED 9174	27.2	8.1	E 33.9
ED 19301	9.2	9.1	W 18.0
ED 37709	350.9	12.9	W 18.3
SCH 1513	13.7	11.1	NA
SCH 3689	8.7	8.4	W 5.0
SCH 9174	25.3	5.6	E 16.6
SCH 19301	16.8	10.1	W 8.5
SCH 33709	4.2	19.7	W 12.6

To further refine the data, and control for annotation error in the previous, larger grouping, Focus Boxes in each image were selected (Figure 9). This reduced the numbers in the data set, focused on N-S trending bedforms, and included junctions that might show change. The pattern that appeared in the first set (full image, Table 2) is seen, in part, here as well: in two of the three sets, NCH and SCH, change occurs in the middle of the time frame. The crest orientations at the end of the set are very similar to that of the first image.

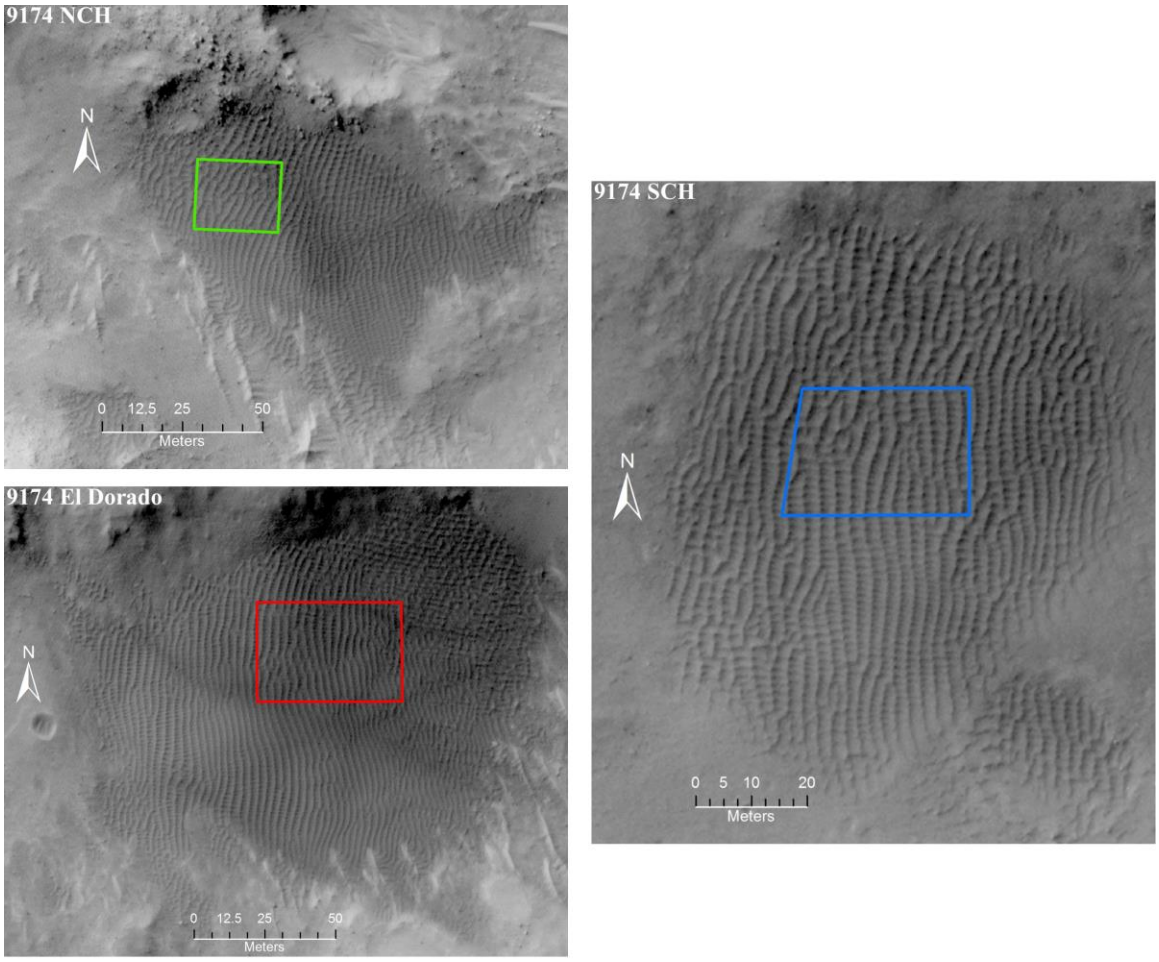

Figure 9. Focus Boxes for each area. The crests within the boxes were redigitized to focus more on N-S trending crests and changing junctions.

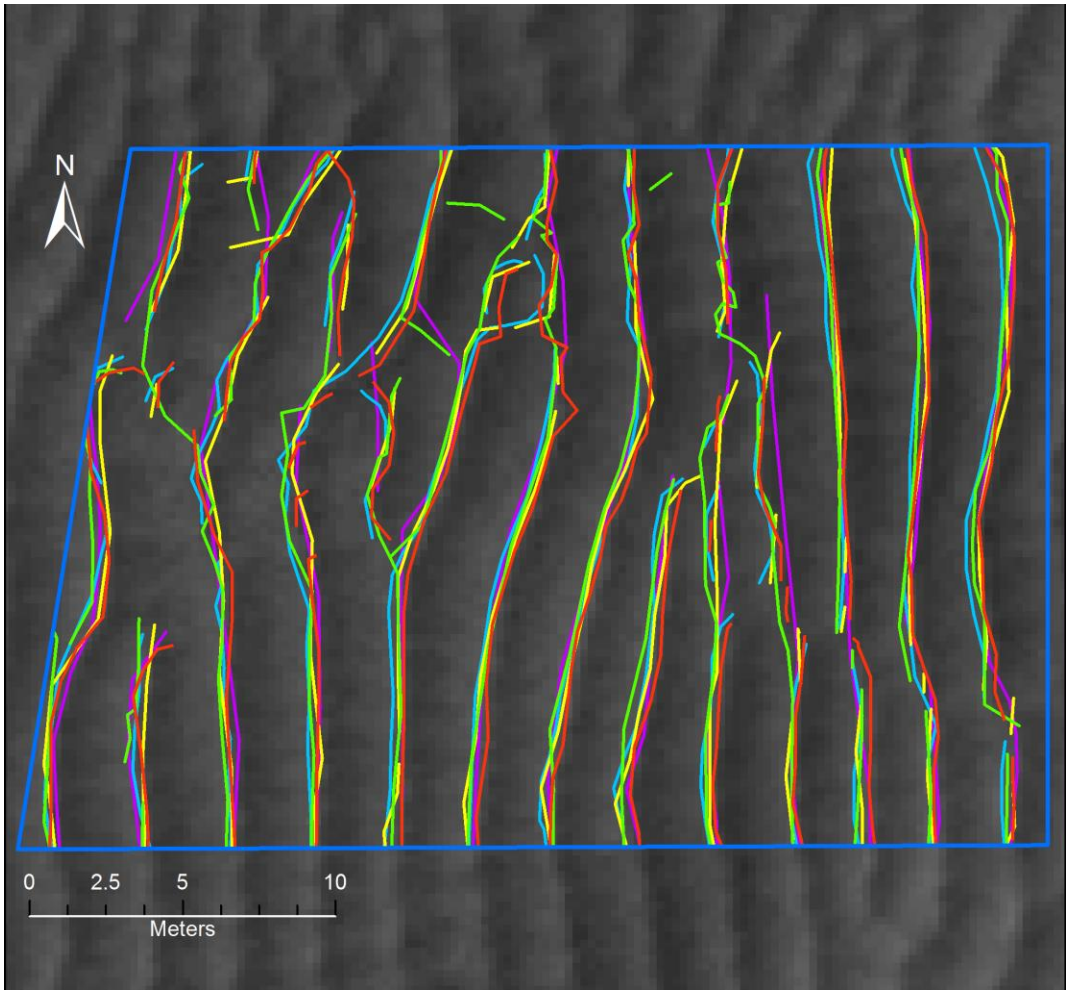

Figure 10. Focus Box crests. All images for SCH area. 1513-red; 3689-green; 9174-yellow; 19301-blue; 33709-violet. Red (earliest image) is mostly seen on the right (east) of each annotated crest, with yellow and blue (following dust events) showing most movement to the left (west). The violet lines most often appear on the east side of the groups, next to red. This tends to confirm the observed movement of the full image and area analyses: maximum movement after the dust storms, and return to near-initial position before the last image.

Table 4

Crest Azimuths for Focus Boxes (3)

Area and Image	Azimuth (deg)	Average Length (m)	Orientation Change
NCH 1513	18.6		
NCH 3689	19.5	6.5	E 0.9
NCH 9174	25.4	5.1	E 5.8
NCH 19301	20.5	6.2	W 4.8
NCH 37709	21.3	8.2	E 0.7
ED 1513	359.7	7.2	
ED 3689	351.3	8.4	W 8.4
ED 9174	0.2	10.2	E 8.6
ED 19301	353.8	7.8	W 6.1
ED 33709	353.4	15.2	W 0.4
SCH 1513	7.5	8.9	
SCH 3689	1.6	9.3	W 5.8
SCH 9174	9.2	5.3	E 7.5
SCH 19301	9.3	8.8	E 0.1
SCH 33709	4.2	14.1	W 4.2

The final crest study identified two crests in each area to track through the images. Figure 11 shows the selected crests and Figure 12 gives an example of the comparison of two crest lines. The disparity between them is not consistent. This may confirm that the digitization is accurate, and that the difference is possibly due to wind gusts. Such winds might be expected within this topographic area, and would be enhanced by the dust storm.

It is possible to see the pixels in this figure; each pixel is equal to 25 cm on the surface, so the two pixel separation represents 0.5 m. Table 5 shows the orientation

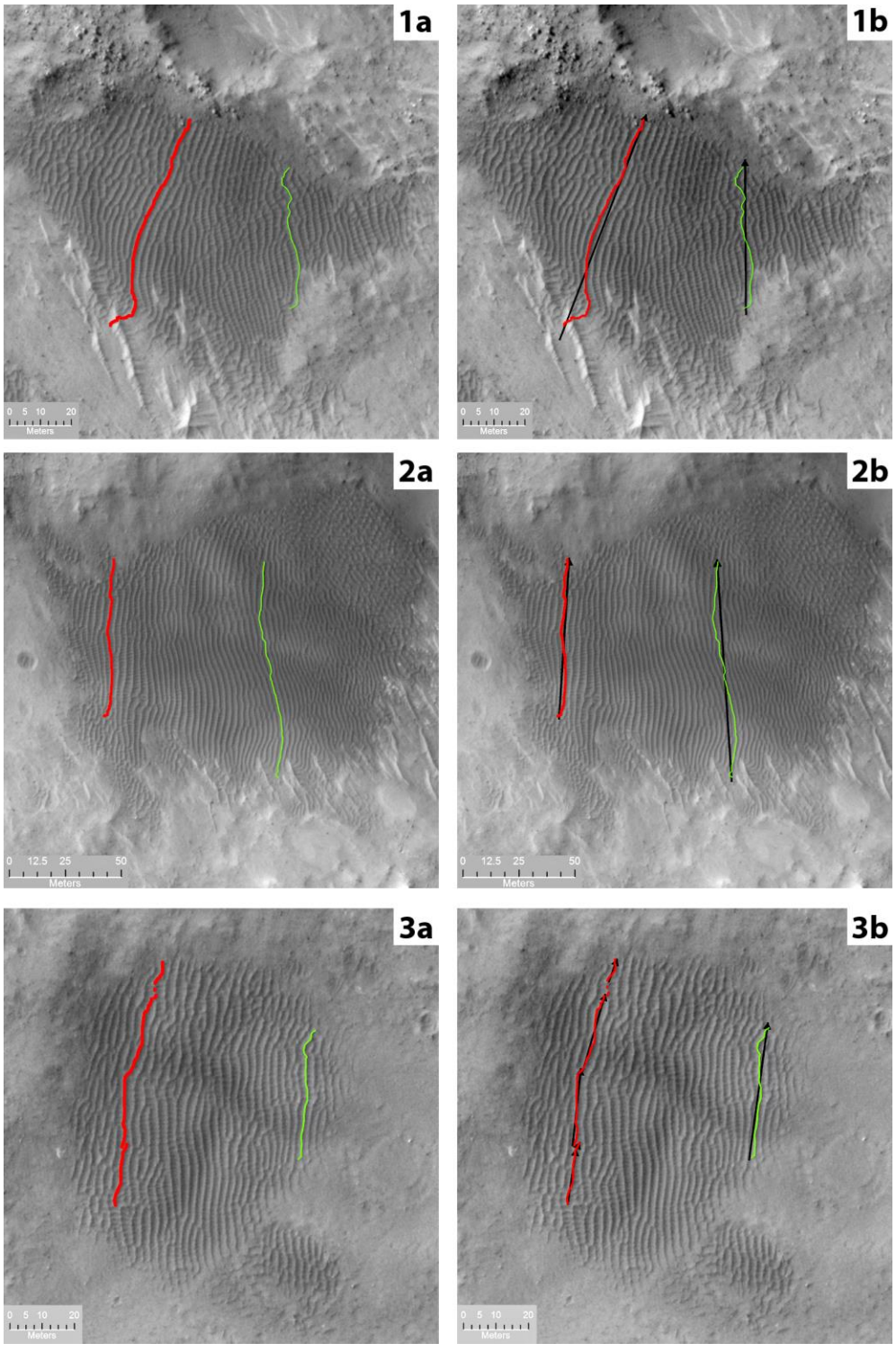

Figure 11. Individual crest study. Examples from image 1513 show the crest choice for all images, and an example of the azimuth determination. 1a and b are NCH, 2a and b are El Dorado and 3a and b are SCH.

Table 5.

Individual Crests(4)

Image	NCH_A	Change (deg)	Ave Length (m)
1513	21.1	NA	78.6
3689	17.2	W3.9	71.9
9174	21.1	E 3.9	79.6
19301	17.1	W 4.1	69.4
37709	16.9	W 0.2	70.2
	NCH_B		
1513	359.7	NA	50.7
3689	359.3	W 0.4	51.1
9174	359.4	E 0.1	51.4
19301	359.5	E 0.1	50.8
37709	359.6	E 0.1	50.0
	ED_A		
1513	356.2	NA	99.9
3689	356.8	E 0.6	97.7
9174	356.4	W 0.4	99.1
19301	356.3	W 0.1	99.6
37709	356.4	E 0.1	99.2
	ED_B		
1513	3.6	NA	72.7
3689	3.4	W 0.2	72.5
9174	3.7	E 0.3	72.6
19301	3.4	W 0.3	72.2
37709	3.3	W 0.1	72.1
	SCH_A		
1513	16.6	NA	11.3
3689	15.3	W 1.3	19.9
9174	16.4	E 1.1	20.2
19301	11.6	W 4.8	41.2
37709	16.6	E 5.0	11.4
	SCH_B		
1513	7.8	NA	43.0
3689	7.8	0	42.9
9174	8.2	E 0.4	43.4
19301	8.5	E 0.3	43.4

change for the individual crests. With the exception of the SCH-B crest, the larger change occurs around image 9174.

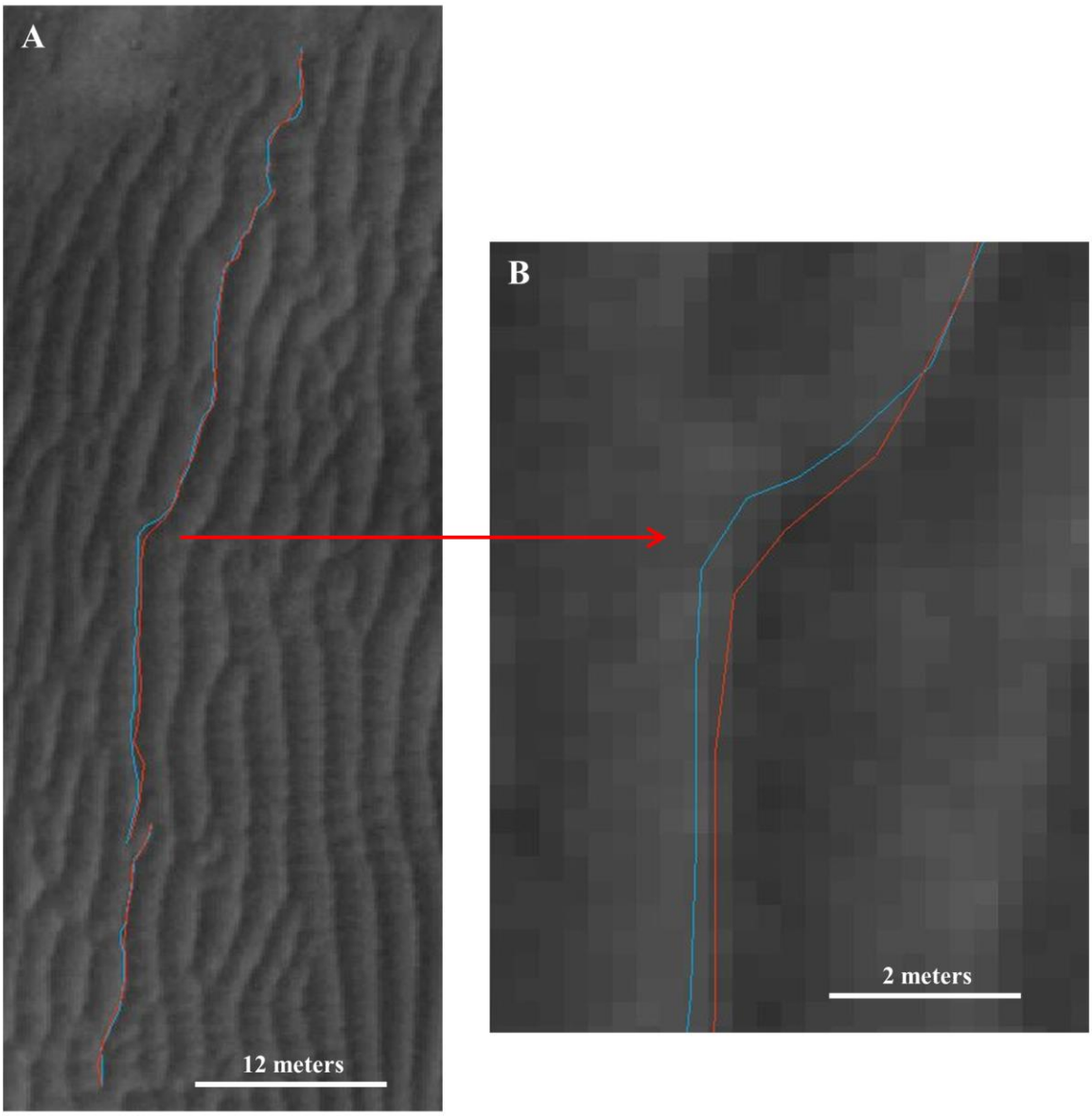

Figure 12. Individual Crest, SCH-A. Two images are overlain: 1513 (red) and 19301 (blue). A shows the complete crestline; B is a closeup of the bend in the middle of the crest. At that point, at least two pixels separate the annotations, possibly indicating movement of ~ 0.5 meters. The base image is PSP_001513.

Individual crest movement was not large, but measurable over the 7.75 year period of the study. Table 6 presents the total pixel movement and the average meters per year. The greatest movement occurred in SCH, with portions Line A moving 3.1 m. The average total movement was approximately two meters, with an annual average movement of 0.25 m.

Table 6

Surface Movement of Individual Crests(4)

Crest	No. Pixels	Meters	M/year
NCH A	7	1.75	0.22
NCH B	6.8	1.7	0.21
ED A	8.6	2.2	0.28
ED B	6.4	1.6	0.20
SCH A	12.2	3.1	0.4
SCH B	5.8	1.45	0.19
Average	7.8	1.97	0.25

DUST DEVIL TRACKS

Dust devil tracks are visible because they siphon dust from the surface, revealing the darker substrate. They reflect two types of daily winds: the prevailing winds predicted in MRAMS, which should be at most 7.75 ms^{-1} , and the winds of thermally-induced vortexes, which can be as much as 17-20 ms^{-1} in a circular direction. While they can be found in nearly still air conditions, they appear to be horizontally driven by the prevailing winds (Greeley, 2004a). An examination of the visible dust devil tracks over the

bedforms in the Columbia Hills shows that the direction of the tracks seems to correlate both with prevailing winds, as predicted by MRAMS, and with the 2007 dust storm and the 2009 regional storm (Wang, 2015), as well as with topography (Ramirez, 2009). The predominant directions of the tracks change in the two images affected by the storms, 9174 and 19301. This is more apparent in two areas, NCH and SCH than in El Dorado. With the bedforms, the final image shows similarities with the first two; this is not the case for the dust devil tracks. Figure 13 gives an example, using the El Dorado images, of how the dust devil tracks were evaluated. It shows tracks in one area for the 7.75 Earth years of the study.

Table 7

Azimuths of Dust Devil Tracks

Area/Image	Number	Azimuth (deg)	Average Length (m)	Change (deg)
NCH 1513	3	134.2	31.2	NA
NCH 3689	2	81.6	44.9	W 52.6
NCH 9174	2	117.8	64.6	E 81.5
NCH19301	5	115.3	38.2	W 2.4
NCH33709	2	112.2	43.7	W 3.1
ED 1513	10	114.6	70.5	NA
ED 3689	8	86.5	55.4	W 28.1
ED 9174	6	81.2	79.5	W 5.2
ED 19301	10	117.9	78.3	E 36.7
ED 33709	2	50.2	98.9	W 67.7
SCH 1513	5	187.5	46.2	NA
SCH 3689	4	286.2	47.2	E 98.6
SCH 9174	6	118.3	40.9	W 167.8
SCH 19301	5	133.4	42.9	E 15.0
SCH 37709	2	92.1	26.7	W 41.2

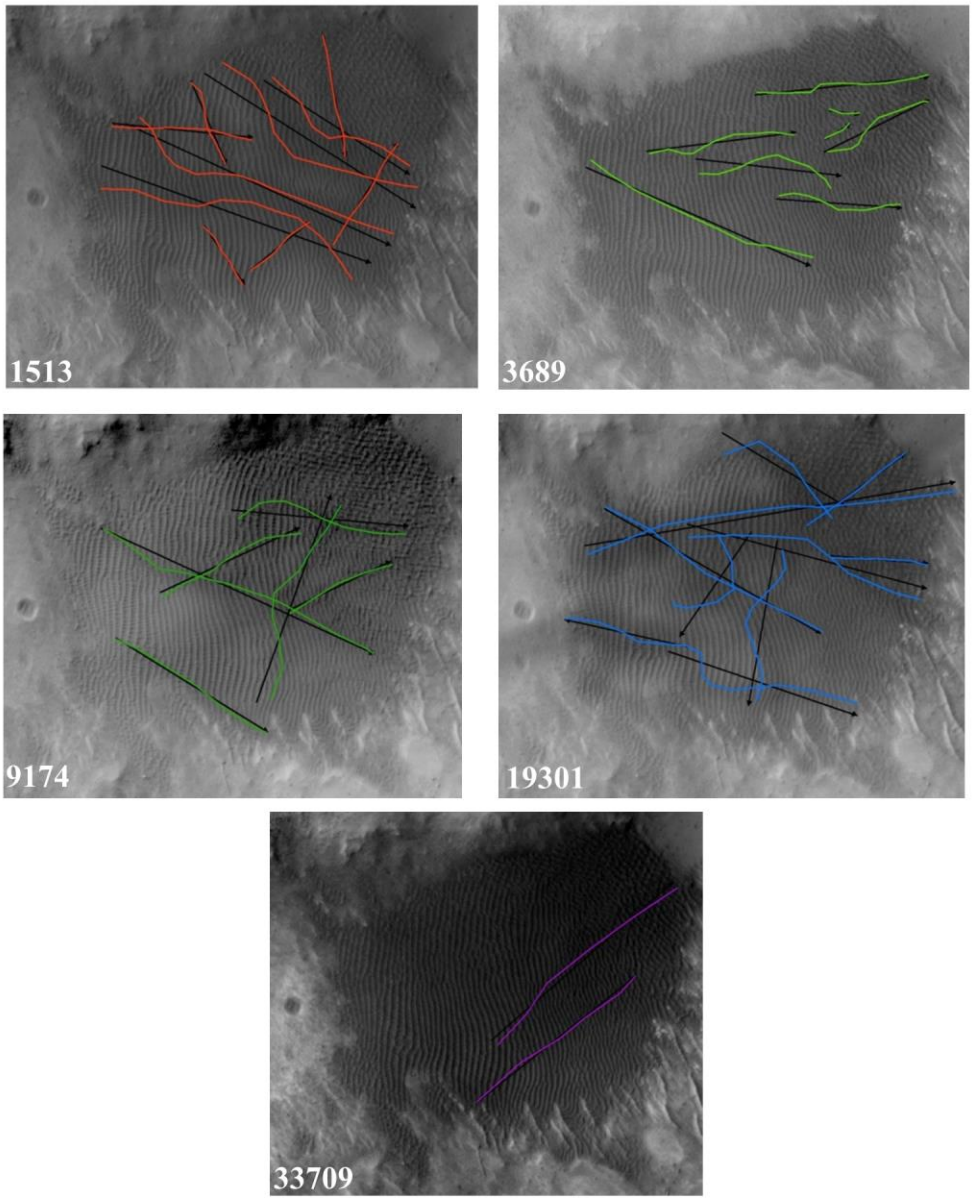

Figure 13. Dust Devil Track Example. Digitized tracks with azimuth determination for each track. El Dorado. Similarities between the first two images, before the dust storm, between the second two, after the dust storm, are apparent. The final image shows new, unexpected orientations.

Rose Diagrams of the dust devil track azimuths (Figure 14) point out the similarities between the two early images with similar ESE orientation, and the two related to the dust storms, with ENE and SSE orientations. This correlates well to the same relationships seen with bedforms. However, whereas the bedforms appear to ultimately revert to the pattern seen in the first images, the final dust devil track image produces an intermediary azimuth (E).

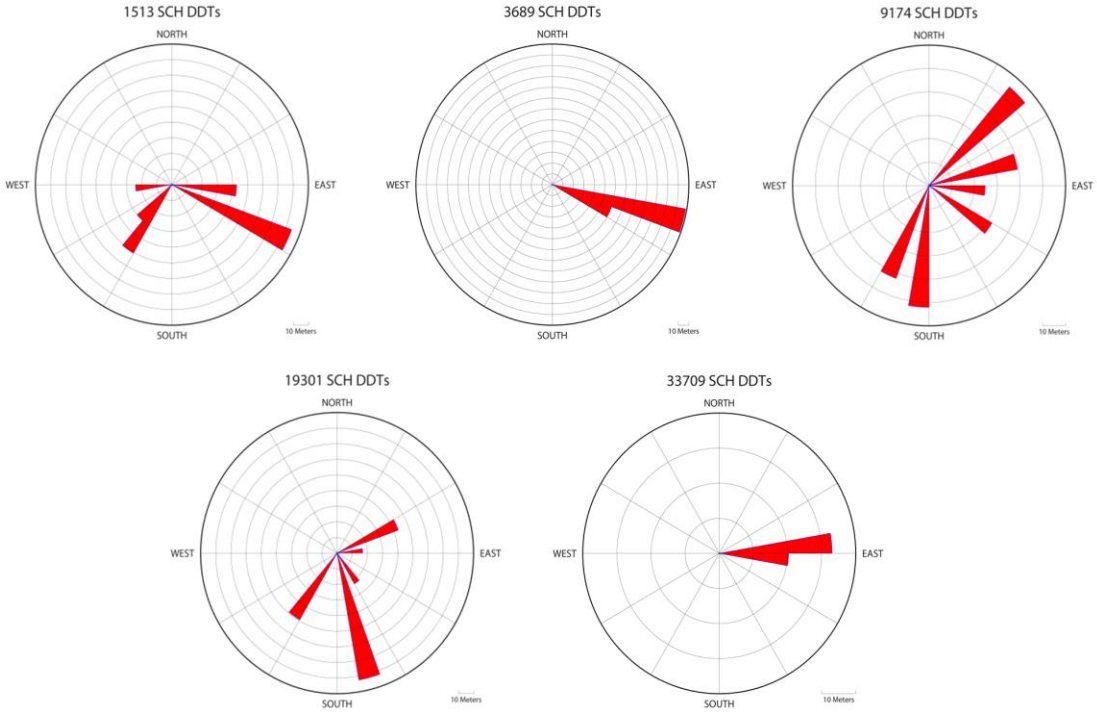

Figure 14. Rose Diagrams of dust devil track azimuths for SCH.

Chapter 4

DISCUSSION AND CONCLUSIONS

BEDFORMS

These transverse bedforms, obviously created by winds, trending mostly N-S, are in slight depressions that all have south-trending slopes of 5-10 degrees. The bedform crests have shown movement by as much as 0.75 m (three pixels) over the period of this study, which reflects four seasons on Mars. In particular, NCH and SCH responded to the global and regional dust storms with the largest change in azimuth orientations being from 3689, before the storm, to 9174, just following the storm, and up to 19301, well after the storm. The movement, however, is not progressive. There is a trend for the crests to return to not far from their original orientation by the final image 33709. The movement tracked by azimuth comparisons shows that the direction of movement is inconsistent; saltating crests would tend to show slipfaces and movement in a single direction. The implication for these bedforms is that saltation is not occurring; the movement more likely reflects reptation or creep. The comparison of individual crests shows that, while the total movement of a crest may be as much as three meters over the study period, the average rate of movement is ~0.25 m. Coincidentally, this is the resolution limit for the HiRISE images. The fact that this set of images produces the highest resolution of the surface yet seen, may serve to confirm the hypothesis that dune and ripple movement has not often been seen due, in part, to the lack of high resolution, repetitve imaging.

ANNOTATION BIAS

Changes observed after the dust storm may be due partly to layering of the dust on the surface. The higher albedo dust may highlight west-east trending bedforms, not normally seen because illumination is from the west. The visually enhanced bedforms might be preferentially digitized, influencing the numerical results. This was observed with the 9174 image, and to a lesser degree with 19301.

The Focus Boxes and Individual Crest studies were added to control some of the effects of preferential annotation. They produced a narrower azimuth range that, with one exception, NCH 33709, confirmed the prior results. The fact that, even in these studies, the two images, 9174 and 19301 (the images showing results of dust storm) generated most of the apparent change, may support the accuracy of the work.

Dust is probably a factor in some error, especially in the complete bedform studies. Figure 15 offers a comparison of a relatively dust-free surface (El Dorado, 3689) to a dust-laden surface (El Dorado, 9174). These are before and after the global dust storm images. The first image is dark, relatively clear of dust; still dust devil tracks can be seen, demonstrating the constant dust fall (Landis, 1996). The second has enough dust to change the appearance of the bedforms; they seem to be smoothed. With the more reflective dust layer, the west-east trending bedforms appear larger. Dust devil tracks are visible on 9174.

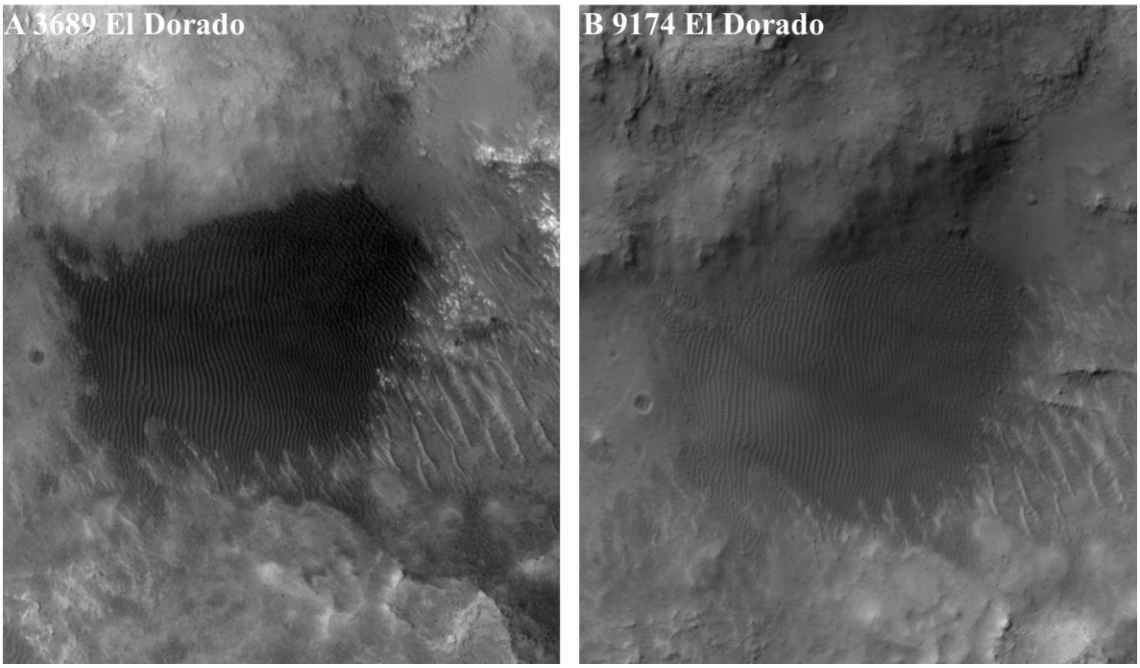

Figure 15 Before and after global dust storm. Dust devil tracks are visible on both images.

IMAGE CHARACTERISTICS

That crests appear to return to near-original position in the final image of the study could be explained by subtle image differences such as in phase and incidence angles, or even the general illumination indicated by solar longitude. Phase angle differences of less than a pixel are apparent between several images, despite the careful registration of the images to small features (rocks, small craters) adjacent to the areas. However, with the size of the features (2.25 - 2.75 meters wide) being quite close to the image resolution (0.25 cm/pixel), the offset could be significant.

Incidence angle and solar longitude both can contribute to errors in interpretation. The height of the sun above the horizon and the general illumination of the surface may skew the appearance of the crests. This is important to note, as, the lower vertical relief

there is for the features, the greater the error can be. The crest orientations of these features, with estimated height of as low as 0.3 m (Sullivan, 2008), might be misinterpreted. This study found crest heights of 1.2m, which might be less vulnerable to misinterpretation.

REGIONAL WINDS

The change in the individual crest orientations is inconsistent in direction over all areas and for each crest within an area, with only one exception, the SCH-B crest. The differences in direction of movement can be seen as confirmation that change is occurring, but not in a sweeping manner more consistent with progressive saltation. The discrepancies may reflect the light, variable winds in the area, and the topographically-influenced winds (Breed, 1979).

Gravity-induced motion may be a reason for the inconsistency in movement direction. Since Spirit identified the materials in El Dorado as "cohesionless grains," they may be induced to slide (creep); as has been noted, the winds may not be inducing saltation.

The apparent return of much of the material to close to its original state may be explained by consistent, alternating winds. MRAMS predicts relatively slow wind speeds of no more than 7.75 ms^{-1} in spring and summer, with much lower speeds in the autumn and winter. The Appendix provides a table of four seasons of wind speeds. These are below the predicted threshold speeds (Greeley and Iverson, 1985). Figure 16 includes four MRAMS plots of wind directions and speeds for Gusev Crater; they represent four

hours in one northern summer day, Ls148. The bimodal winds are apparent, and appear to be influenced by slope winds, caused by the crater rims, Ma'adim Vallis, and Apollinaris Patera, and local heating, on the plains in the center of the crater (Greeley, 2003). At A, 00:69 Local Mean Time (LMT), the winds come into Gusev from Ma'adim Vallis at the highest speeds, up to 7.75 ms^{-1}, flowing SE to NW. By 08:70 (B), the winds are reduced; more air is moving N-S and NE-SW, indicating a shift toward movement from the center of the crater to the edges. At 13:70, (C), the airflow is from the crater center outward in all directions, with a core of very low speeds, an indicator of diurnal heating, NW of the center. By 20:70 (D), the winds have reverted to the nighttime flow from the Ma'adim Vallis (SE-NW). There are notable seasonal variations as well: wind speeds are slightly higher at night during northern spring and summer, and higher during the day during autumn and winter (see Appendix). These relatively low speed winds are clearly bimodal; small, symmetrical bedforms, as those seen here, are predictable.

SYMMETRY OF THE BEDFORMS

The crests on the edge of El Dorado, examined by Spirit, were thought to show slipfaces. At that location, on the NE edge of the field, the bedforms are probably influenced by the topographic winds (Hobbs, 2010), and could develop slipfaces. However, after examining all the crests from above, and noting the symmetry of the dark and light pixels surrounding the crests, it appears that the great majority of bedforms in the Columbia Hills are symmetrical, showing no slipfaces. They are indeed small: approximately 1.2m high and with average wavelengths of 2-3m. On Earth, symmetrical

ripples may be seen in lacustrine, shoreline environments, but are likely to be only a few centimeters tall, with wavelengths up to tens of centimeters. At this location on Mars, regular, gentle winds seem to be capable of producing this larger, subaerial, form.

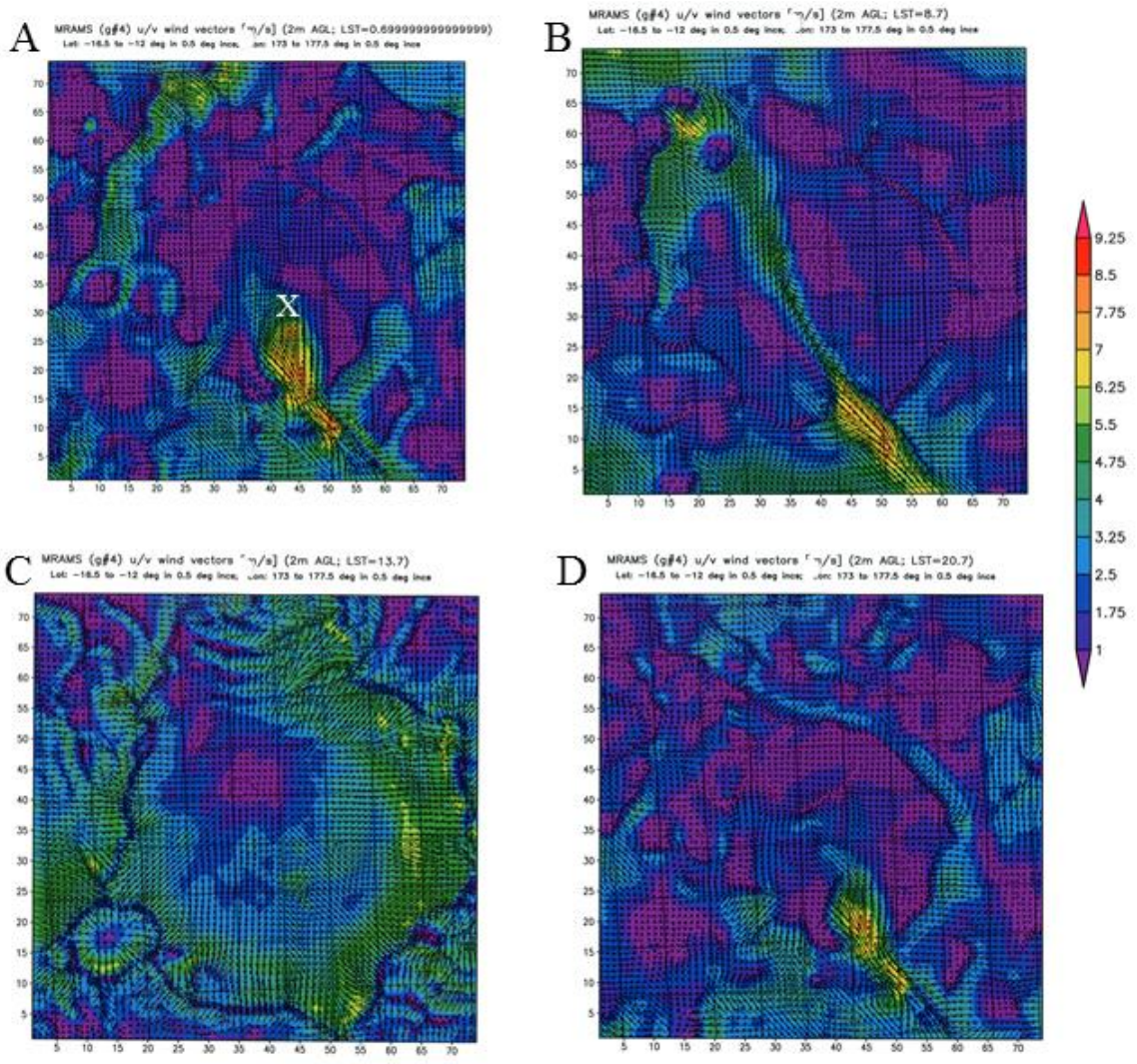

Figure 16. MRAMS winds speeds and directions for Gusev Crater. The location of the Columbia Hills is marked with the X in image A. *(Rafkin, 2001)*

CONSIDERATION OF DUST DEVIL TRACKS

The dust devil tracks show more obvious effects of both regular winds and those associated with dust storms. Two of the three areas, NCH and ED, have similar direction of change, while the SCH results are different for the two image sets which represent the dust storms. SCH is located at the bottom of the Columbia Hills and central to the two ridge extensions of the hills; it is exposed to wind directions that may be even more variable than experienced in the other two areas.

That dust devil tracks are seen in the Columbia Hills is remarkable. On Earth, dust devils are found on plains and are seen to dissipate when encountering small obstacles, such as boulders and plants. This study provides evidence of dust devil activity on Mars within hills and at elevations of ~120 m above the crater floor. Further, since dust devils are not known to form in hills, these tracks probably represent the signature of dust devils forming on the plains to the west; they have traveled over half of the obstacle structure of the Columbia Hills and appear to have continued beyond the bedforms they have crossed. This dust devil behavior is, as yet, unexplained.

DUST STORMS

The global storm of 2007 and a regional one of lesser impact in 2009 (Wang, 2015) had obvious effects on both the bedforms and the dust devil tracks in the Columbia Hills. The magnitude of azimuth change was greatest for both feature types during those periods. Both types appear to have a “normal” or “start” position, shown in the first two images, which, although disrupted by the storms, returned within two years of the larger

storm. This may imply a current climate pattern, which would be well-represented by MRAMS.

CONCLUSIONS

There is abundant evidence of wind-driven modifications to the Columbia Hills bedforms. It supports the concept of current winds on Mars moving, but perhaps not saltating, particles of many sizes. There are caveats with regard to this research, and any similar work that uses image sources that are very close to the size of the features being studied. The dust-sand conundrum of the past 40 years is being tackled by computer modeling as well as orbital studies, such as this one. As modelers refine threshold speeds, and orbiting instruments produce even better resolution images, we may expect to see that particles in the entire size range from dust to coarser sand may be lofted on Mars.

Dust devils on Mars are regularly influenced by regional winds, powered by storms, and are able to breach substantial obstacles. Aspects of this study may contribute to a better understanding of the function and power of winds in low-gravity, thin atmosphere of Mars, confirming the effect of light but regular winds. The results of this study reflect the influence of topography as well as regional and global winds over this relatively small area, and lend support to the MRAMS model.

The small coherent bedforms in the Columbia Hills are of a size not previously studied; while features this size have been observed, they are identified as secondary features to larger bedforms. The changes to the fine basaltic sand bedforms of the Columbia Hills appear to correspond to both modest bimodal winds as well as to

significant dust storms. Movement such as this, probably with little saltation, may demonstrate an intermediate behavior, between dust and coarse sand, that contributes to the resolution of the dust-sand conundrum.

REFERENCES

Bagnold, R. A. (1954). *The physics of blown sand and desert dunes*. New York: Dover Publications, NY.

Balme, M, Berman, D.C., Bourke, M.C., Zimbelman, J.R. (2008). Transverse aeolian ridges (TARs) on Mars. *Geomorphology 101,* 703-720, doi:10.1016/j.geomorph.2008.03.011.

Bandeira, L., J.S. Marques, J. Saraiva, P. Pina. (2010). Martian dune fields detection by automated approaches. *2nd International Planetary Dunes Workshop* Abstract #2021.

Bourke, M.C., N. Lancaster, L.K. Fenton, E.D.R. Parteli, J.R.Zimbelman, J. Radebaugh. (2010). Extraterrestrial dunes: An introductions to the special issue on planetary dune systems. *Geomorphology, 121, 1-2,* 1-14, doi:10.1016/j.geomorph.2010.04.007.

Bourke, M.C., Edgett, K.S., Cantor, B.A. (2008). Recent aeolian dune change on Mars. *Geomorphology 94,* 247-255, doi:10.1016/j.geomorph.2007.05.012.

Bridges, N.T. (2007). Windy Mars: A dynamic planet as seen by the HiRISE camera. *Geophysical Research Letters, 34* (L23205), doi.10.1029/2007GL031445.

Bridges, N.T., M.C. Bourke, P.E. Geissler, M.E. Banks, C.Colon, S. Diniega, et al. (2012). Planet-wide sand motion on Mars. *Geology, 40, 1,* 31-34, doi:10.1130/G32373.1.

Breed, C.S. and M.J. Grolier and J.F. McCauley. (1979). Morphology and distribution of common 'Sand' dunes on Mars: Comparison with the Earth. *Journal of Geophysical Research, 84,* B14, 8183-8204.

Chojnacki, M, Burr, D.M. and Moersch, J.E. (2010). Evidence of bed form deflation, modification and transport at Endeavour Crater, Meridiani Planum, Mars, from orbital observations. *2nd International Planetary Dunes Workshop* Abstract #2028.

David, Leonard.(2005). "Spirit gets a dust devil once-over." *Space.com.* www.space.com/861-spirit-dust-devil.html, Retrieved July 14, 2013.

Edgett, K.S. and Malin, M.C. (2000). New views of Mars eolian activity, materials, and surface properties: Three vignettes from the Mars Global Surveyor Mars Orbiter Camera., *Journal of Geophysical Research, 105,* E1, 1623-1650.

Ewing, R.C. (2016). Dune ripples on Earth and Mars. Accessed July 30, 2016, from https://planetarygeomorphology.wordpress.com/2016/07/30/dune-ripples-on-earth-and-mars/.

Fenton, L.K. and R. K. Hayward. (2010). Southern high latitude dune fields on Mars: Morphology, aeolian inactivity, and climate change. *Geomorphology 121, 1-2,* 98-121, doi:10.1016/j.geomorph.2009.11.006.

Fenton, L.K. (2006). Dune migration and slipface advancement in the Rabe Crater dune field, Mars. *Geophysical Research Letters, 33*, L20201, doi:10.1029/2006GL027133.

Fenton, L.K., Toigo, A.D., Richardson, M.I. (2005). Aeolian processes in Proctor Crater on Mars: Mesoscale modeling of dune-forming winds. *Journal of Geophysical Research, 110,* E06005, doi:10.1029/2004JE002309.

Gierasch, P. and Sagan, C. (1971). A preliminary assessment of martian wind regimes .*Icarus 14*, 312-318.

Golitsyn, G.S. (1973). On the Martian dust storms. *Icarus, 18,* 113.

Grant, J.A., R.E. Arvidson, J.F. Bell III, N.A. Cabrol, M.H. Carr, P. Christensen, et al. (2004). Surficial deposits at Gusev Crater along Spirit rover traverses. *Science, 303, 5685,* 807-810, doi:10.1126/Science.1099849.

Greeley, R., D.A. Waller, N.A. Cabrol, G.A. Landis, M.T. Lemmon, LD.V. Neakrase, et al. (2010). Gusev Crater, Mars: Observations of three dust devil seasons. *Journal of Geophysical Research, 115,* E00F02, doi:10.1029/2010JE003608.

Greeley, R., P.L. Whelley, R.E. Arvidson, N.A. Cabrol, D.J. Foley, B.J. Franklin, et al. (2006). Active dust devils in Gusev crater, Mars: Observations from the Mars Exploration Rover Spirit. *Journal of Geophysical Research, 111, E12S09*, doi:10.1029/2006JE002743.

Greeley, R., R. Arvidson, J.F. Bell III, P. Christensen, D. Foley, A. Haldemann, et al. (2005). Martian variable features: New insight from the Mars Express Orbiter and the Mars Exploration Rover Spirit. *Journal of Geophysical Research, 110,* E06002, doi:10.1029/2005JE002403.

Greeley, R., R.E. Arvidson, P.W. Barlett, D Blaney, N.A. Cabrol P.R. Christensen, et al. (2004). Wind-related processes detected by the Spirit rover at Gusev Crater, Mars. *Science, 305,* 817-821.

Greeley, R., P.L. Whelley and L.D.V. Neakrase. (2004a). Martian dust devils: Directions of movement inferred from their tracks. *Geophysical Research Letters, 31*, L24702, doi:10.1029/2004GL021399.

Greeley, R., R.O. Kuzmin, S.C.R. Rafkin, T.I. Michaels, R. Haberle. (2003). Wind-related features in Gusev crater, Mars. *Journal of Geophysical Research, 108*, E12, 8077, doi:10.1029/2002JE002006, 2003.

Greeley. R., M.D. Kraft, R.O. Kuzmin, N.T. Bridges. (2000). Mars Pathfinder landing site: Evidence for a change in wind regime from lander and orbiter data. *Journal of Geophysical Research,105, E1*, 1829-1840, doi:10.1029/1999JE001072.

Greeley, R., and Iverson, J.D. (1985). *Wind as a geological process on Earth, Mars, Venus and Titan*. Cambridge: Cambridge Planetary Science, 4, Cambridge University Press.

Haberle, R.M., J.B. Pollack, J.R. Barnes, R.W. Zurek, C.B. Leovy, J.R. Murphy, et al., (1993). Mars Atmospheric Dynamics as Simulated by the NASA Ames General Circulation Model. *Journal of Geophysical Research, 98*, E2, doi: 10.1029/92JE02946.

Hayward, R.K.,L..K. Fenton, K.L. Tanaka, K.F. Mullins, T.N.Titus, M.C. Bourke. (2008). Mars Global Digital Dune Database and initial science results. *Journal of Geophysical Research, 112*, E11007, doi:10.1029/2007JE001943.

Hayward, R.K., L.K. Fenton, T.N. Titus. (2014). Mars Global digital Dune Database (MGD^3): Global dune distribution and wind pattern observations. *Icarus 230*, 38-46, doi: 10.1016/j.icarus.2013.04.011.

Hobbs, S.W, D.J. Paull, M.C. Bourke. (2010). Aeolian processes and dune morphology in Gale Crater. *Icarus 210,* doi:10.1016/j.icarus.2010.06.006.

Kienenberger, R. (2011). Distribution of windblown sediment in small craters on Mars. (Masters thesis, Arizona State University, 2011).*Proquest Dissertation Publishing,* 1491007.

Kok, J.(2010). Difference in the wind speeds required for initiation versus continuation of sand transport on Mars: Implications for dunes and dust storms. *Physical Review Letters, 104,* 074502, doi: 10.1103/PhysRevLett.104.074502.

Landis, G. (1996). Dust Obscuration of Solar Arrays. *Acta Astronautica, 38,* 11, 885-891.

Lapotre, M.G,.A., R.C. Ewing, M.P. Lamb, W.W. Fischer, J.P. Grotzinger, D.M. Rubin, et al. (2016). Large wind ripples on Mars: A record of atmospheric evolution. *Science, 353, 6294,* 55-58, doi:10.1126/science.aaf3206.

Malin, M.C., M.H. Carr, G.E. Danielson, M.E. Davies, W.K. Hartman, A.P. Ingersoll, et al. (1998). Early Views of the Martian Surface from the Mars Orbiter Camera of Mars Global Surveyor. *Science 279*, 1681.

McEwen, A.S., E.M. Eliason, J.W. Bergstrom, N.T. Bridges, C.J. Hansen, W.A. Delamere. (2007). Mars Reconnaissance Orbiter's High Resolution Imaging Science Experiment (HiRISE). *Journal of Geophysical Research, 112*(E05S02), doi:10.1029/2005JE002605.

Parteli, E.J.R., M.P. Almeida, O Duran, Jose S. Andrade Jr., H.J.Herrmann. (2009). Sand transport on Mars. *Computer Physics Communications 180*, 609-611.

Pollack, J.B., R. Haberle, R. Greeley and J. Iversen. (1976). Estimates of the wind speeds required for particle motion on Mars. *Icarus 29*, 395-417.

Rafkin, S.C.R., T.M. Haberle, T.I. Michaels. (2001). The Mars Regional Atmospheric Modeling System: Model description and selected simulations. *Icarus 151*, 228-256, doi:10.1006/icar.2001.6605.

Ramirez, R. (2009). Numerical and geomorphic analysis of topographic effects on martian dust devils (Doctoral dissertation, Arizona State University, 2009).

Sagan, Carl, J. Veverka, P. Fox, R. Dubisch. (1972).Variable features on Mars: Preliminary mariner 9 television results. *Icarus 17*, 2, pp. 346-372.

Sagan, C. and Pollack, J.B. (1969). Windblown dust on Mars. *Nature 223*, 791-794.

Silvestro, S., L.K. Fenton, D.A. Vaz, N. Bridges, G.G. Ori. (2010). Ripple migration on active dunes in Nili Patera (Mars). *2nd International Planetary Dunes Workshop* Abstract #2003.

Silvestro, S., D.A. Vaz, R.C. Ewing, A.P. Rossi, L.K. Fenton, T.I. Michaels. (2013). Pervasive Aeolian activity along rover Curiosity's traverse in Gale Crater, Mars. *Geology, 41, 4*, 483-486, doi:10.1130/G34162.1.

Squyers, S.W., R.E. Arvidson, J.F. Bell III, J. Bruckner, N.A. CabrolW. Calvin, et al. (2004). The Spirit Rover's Athena science investigation at Gusev Crater, Mars. *Science, 305*, 794-799, doi:10.1126/science.3050794.

Sullivan, R., R. Greeley, M. Kraft, G. Wilson, M.Golombek, K. Herkenhoff, et al. (2000). Results of the Imager for Mars Pathfinder windsock experiment. *JGR 105*, E10,24,547-24,562.

Sullivan, R., R. Arvidson, J.F. Bell III, R. Gellert, M.Golombek, R. Greeley, et al. (2008). Wind-driven particle mobility on Mars: Insights from Mars Exploration Rover observations at "El Dorado" and surroundings at Gusev Crater. *Journal of Geophysical Research, 113, E06S07*, doi:10.1029/2008JE003101.

Verba, C., P.E. Geissler, T.N. Titus, D. Waller. (2010). Observations from the High Resolution Imaging Science Experiment (HiRISE): Martian dust devils in Gusev and Russell craters. *Journal of Geophysical Research, Planets, 115, E9*, doi: 10.1029/2009JE003498.

Waller, D. (2011). Active dust devils on Mars: A comparison of six spacecraft landing sites. (Master's thesis, Arizona State University, 2011). *Masters Abstracts International, 49-05,* 138.

Wang, H. and M.I. Richardson. (2015). The origin, evolution, and trajectory of large dust storms on Mars during Mars years 24-30 (1999-2011). *Icarus, 251,* 112-127, doi.org/10.1016/j.icarus.2013.10.033.

Wilson, I.G. (1971). Desert sandflow basins and a mode for the development of ergs. *The Geographical Journal, 137, 2,* 180-199.

Zimbelman, J.R. (2010). Transverse aeolian ridges on Mars: First results from HiRISE images. *Geomorphology, 121*, pp. 22-29.

Zimbelman, J.R. (2000). Non-active dunes in the Archeron Fossae region of Mars between the Viking and Mars Global Surveyor eras. *Geophysical Research Letters, 27*, 7, 1069-1072.

APPENDIX

MRAMS SEASONAL PREDICTED WIND SPEEDS

FOR GUSEV CRATER

Seasonal Predicted Windspeeds for Gusev Crater*

	Spring Ls 058		Summer Ls 148	
LMT	Azimuth	Speed (m/sec)	Azimuth	Speed (m/sec)
0.69	160	3.25-4.0	340	4.0-4.75
1.7	159	4.75-5.50	152	2.50-4.0
2.7	155	5.50-6.25	144	2.50-3.25
3.7	135	3.25-4.0	145	3.25-4.0
4.7	132	1.75-2.50	144	4.75-5.50
5.7	132	1.75-2.50	140	2.50-4.0
6.7	138	2.50-3.25	140	1.75-2.50
7.7	155	4.0-4.75	110	1.0-2.50
8.7	195	2.50-3.25	38	1.0-1.75
9.7	270	1.75-2.50	185	1.0-2.50
10.7	330	1.75-2.50	185	1.0-1.75
11.7	318	1.0-1.75	167	1.0-1.75
12.7	312	< 1.0	272	1.75-2.50
13.7	320	1.0-1.75	330	2.50-3.25
14.7	270	2.50-3.25	305	3.25-4.0
15.7	280	2.50-3.25	300	3.25-4.0
16.7	185	1.0-1.75	320	1.0-1.75
17.7	185	< 1.0	275	< 1.0
18.7	183	1.0-1.75	212	< 1.0
19.7	185	< 1.0	132	< 1.0
20.7	185	1.0-1.75	147	1.75-2.50
21.7	183	2.50-3.25	157	4.75-6.25
22.7	162	4.0-4.75	157	4.0-4.75
23.7	158	5.50-6.25	160	3.25-4.0

	Autumn Ls 238		Winter Ls 328	
	Azimuth	Speed (m/sec)	Azimuth	Speed (m/sec)
0.69	124	1.0-1.75	135	< 1.0
1.7	145	1.0-1.75	128	< 1.0
2.7	280	1.0-1.75	135	1.0-1.75
3.7	136	< 1.0	183	1.0-1.75
4.7	175	2.50-3.25	189	1.0-1.75
5.7	166	2.50-3.25	164	1.0-1.75

6.7	148	1.0-2.50	153	1.0-1.75
7.7	235	1.0-2.50	135	1.0-1.75
8.7	274	< 1.0	267	1.0-1.75
9.7	278	< 1.0	218	< 1.0
10.7	238	< 1.0	285	< 1.0
11.7	190	1.0-1.75	257	< 1.0
12.7	320	2.5-4.0	225	1.0-1.75
13.7	330	4.0-4.75	355	1.0-1.75
14.7	358	2.50-3.25	320	2.50-3.25
15.7	300	4.0-4.75	339	3.25-4.0
16.7	320	3.25-4.75	322	2.50-3.25
17.7	305	1.75-2.50	345	2.50-3.25
18.7	378	< 1.0	360	1.0-1.75
19.7	252	1.0-2.50	338	1.75-2.50
20.7	240	1.75-2.50	235	1.75-2.50
21.7	225	1.0-1.75	235	1.0-1.75
22.7	130	1.0-1.75	246	< 1.0
23.7	138	1.0-1.75	158	1.0-1.75

*LMT: Local Mean Time

Black: SE-NW winds

Red: NW-SE winds

Blue: highest wind speeds